Available online at www.sciencedirect.com

ScienceDirect

Energy Procedia 42 (2013) 587 – 596

Energy Procedia

The Mediterranean Green Energy Forum 2013, MGEF-13

A Comparison Between Static and Dynamic Performances of a Z-source and a Dual-Stage Boost Converter Under SMC for PV Energy Applications

A. El Aroudi[1], R. Haroun[1], A. Cid-Pastor[1], A. Kouzou[2] and L. Martínez-Salamero[1]

Departament d'Enginyeria Electrònica, Elèctrica i Automàtica,
Escola Tècnica Superior d'Enginyeria,
Universitat Rovira i Virgili,
Tarragona, Spain
Email addresses: {abdelali.elaroudi,reham.haroun,angel.cid,luis.martinez}@urv.cat
[2]*University of Djelfa, Djelfa, Algeria*
Email address: kouzouabdellah@ieee.org

Abstract

A comparative study is carried out for the static and dynamic performances of a Z-source converter and a cascade interconnection of two DC-DC boost converters in their potential use for high conversion ratio PV energy applications. A Sliding-Mode Control (SMC) is used for both systems which are operated at the same conditions. Their stability analysis is carried out and their efficiency are compared analytically and validated by numerical simulations using PSIM software. It is shown that the dual-stage boost converter outperforms and the Z-source converters when used in impedance matching between a PV generator and a resistive load.

Keywords: Dual-stage boost converter, Z-source converter, PV energy applications, Impedance matching.

1. Introduction

For facing the different energy sector challenges in an economically efficient way, the first step is to maximize the use of resources by improving the ways of generating, managing and consuming electricity. Recently, an increased interest is shown in clean Renewable Energy Resources (RESs) due to concerns about global warming and its related harmful greenhouse effect, air quality and sustainable development [1]. It is foreseen that in the future power grid, not only the utilities, but also the users can produce electric energy by aggregating Distributed Generation Sources (DGS) [2] such as Wind Farms (WF) Photovoltaic (PV) panels and Fuel Cells (FC). In that context, solar arrays, wind turbines and batteries are used to feed the main dc bus, as well as the utility grid and plug-in hybrid electric vehicles forming the so-called microgrid system [3] (Fig.1). The microgrid can either work in the stand-alone mode or be connected to the utility grid performing peak shaving and smooth transitions between the different modes of operation. In the microgrid context, the future home electric system is foreseen to have two dc voltage levels: a high dc voltage (380 V) powering major home appliances and electric vehicle charging and a low dc voltage (48 V) for supplying computer loads, low power consumer electronics, lighting etc... As a way to overcome ac distribution problems, dc microgrids are discussed and analyzed as a solution for new ways of power distribution. For instance, in [4], the authors evaluated

doi:10.1016/j.egypro.2013.11.060

a dc distribution system in a commercial facility with different supply voltages comparing the energy losses of the dc system with those of an ac power system. The authors found that, at the highest voltage level, dc distribution can be more beneficial, from both economic and technical standpoints. In [5], a comparison between operating characteristics has been carried out between a dc and an ac distribution system that have been created to supply energy for an office laboratory setup with several loads. It has been concluded that the dc distribution system can be preferable to the ac system in applications with many electronic loads, because dc distribution can provide higher power quality.

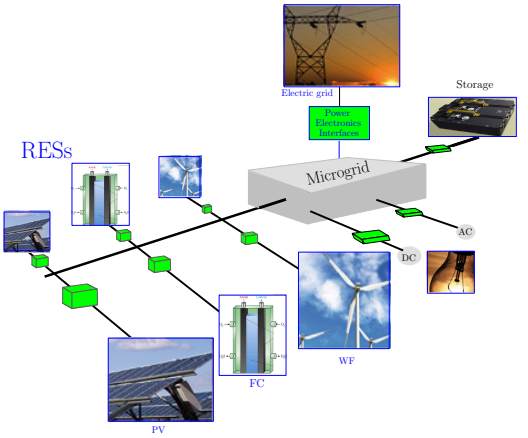

Figure 1. Microgrid supplied from renewable energy resources (RESs).

The photovoltaic technologies have rapidly expanded during the last decades and it is foreseen that they will significantly increase the proportion of solar energy use, which can be considered as the most promising green energy of the new century due to its abundance [6, 7]. However, the major problem of energy generation from this important energy source is the optimal operation of the PV panels.

For domestic PV application, new residential scale photovoltaic (PV) arrays are commonly connected to the grid by two approaches. The first one consists of connecting a series string of PV panels to the converters. The second one consists of connecting a panel per converter. The panel-per-converter approach offers many advantages like individual panel Maximum Power Point Tracker (MPPT), which gives great flexibility in panel layout, replacement, and insensitivity to shading, better protection of PV sources and redundancy in the case of source or converter failure, easier and safer installation and maintenance and better data gathering [8]. In this kind of applications, high conversion ratio are needed to convert the low voltage of the PV panel to the dc bus voltage. A typical problem in electrical power generation using PV systems is increasing the output voltage from a dc voltage of the PV panel (18 V) to a higher voltage of about 400 V which is required by the output bus (Fig.2). The problem can be handled either by using a simple step-up converter with high duty cycle or by using cascaded converters or a step-up transformer. The use of a single stage in performing this conversion ratio will imply working with high duty cycles and therefore will increase the losses which will in turn jeopardize the system efficiency and reduce the voltage conversion ratio. Moreover, the use of an individual power converter with a high duty cycle to obtain high voltage conversion ratios has some design limitations due to the finite commutation times of the power devices and the size of the passive elements. Besides, the use of a step-up transformer limits the operating frequencies and increases the problems of switching surges. If galvanic isolation is not required, the cascade connection of two boost converters can be a good alternative to obtain high voltage step-up ratios. One of the most widely studied combination of switched-mode power converters could be the cascade connection of converters with the aim of obtaining these high voltage conversion ratios. For that, it is necessary to have an adaptation stage with high voltage conversion ratio in addition to good static and dynamic performances. Recently, the Z-source converter has been proposed as an efficient way of obtaining high conversion ratio with relatively low values of the duty cycles. The Z-source converter is a power converter with both buck and boost capabilities which has been first proposed in 2002 [9]. The Z-source converter has been recently studied and investigated by several researchers [10]. Therefore, in this paper, a comparative study will be carried out for the

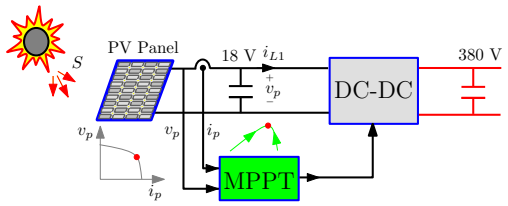

Figure 2. Grid connected PV panel through a DC-DC conversion stage.

dynamic and static performances of a dual-stage boost converter and the Z-source converter. Both systems will be used to obtain a conversion ratio of about 25.

The aim of this paper is to perform a comparative study between the dual-stage boost converter and the Z-source converter under sliding mode control (SMC) for their potential used in impedance matching in PV energy applications. The two cascaded boost converters and the Z-source converter will be used to supply a load resistance with 380 V dc from a low dc voltage source that represents the voltage of a PV panel. It will be shown the two cascaded boost converters outperforms the the Z-source converter in terms of both stability and efficiency.

The rest of the paper is organized as follows: Section 2 presents the dynamic performances of a dual-stage boost and Z-source converters under SMC. The ideal sliding dynamics, the mathematical continuous-time model, the equilibrium point and the stability analysis of both systems will be presented in the same section. Section 3 deals with numerical simulations to validates the theoretical predictions for both systems and a comparison in terms of stability is carried out. In Section 4, the static performances such as efficiency, size and cost are discussed. Finally, some concluding remarks of this work are summarized in the last section.

2. Dynamic performances

2.1. The dual-stage boost converter under sliding-mode control

Fig. 3 depicts a possible practical implementation of a dual-stage DC-DC boost converter under SMC. The circuit in Fig. 3 consists of two boost converters with two sliding surfaces, one surface for each converter. The first surface is described by the switching function $s_1(x) = g_1 V_g - i_{L1}$ for the first stage, which establishes the steady state relationship between the input voltage V_g and the input current i_{L1} where $g_1 = 1/r_1$. The second surface for the second stage is described by the switching function $s_2(x) = g_2 v_{c1} - i_{L2}$ which establishes the relationship between the intermediate voltage v_{c1} and the intermediate current i_{L2} where $g_2 = 1/r_2$.

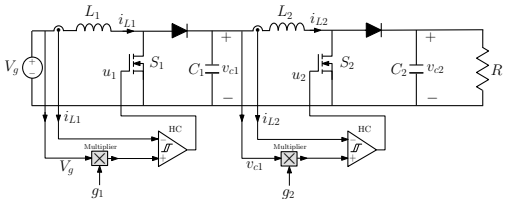

Figure 3. Schematic diagram of a dual-stage boost converter under SMC.

2.1.1. Switched model

By applying standards KVL and KCL to the circuit depicted in Fig. 3, the following set of differential equations describing the system dynamical behavior is obtained

$$\frac{\mathrm{d}i_{L1}}{\mathrm{d}t} = \frac{V_g}{L_1} - \frac{v_{c1}}{L_1}(1-u_1) \quad (1)$$

$$\frac{\mathrm{d}i_{L2}}{\mathrm{d}t} = \frac{v_{c1}}{L_2} - \frac{v_{c2}}{L_2}(1-u_2) \quad (2)$$

$$\frac{\mathrm{d}v_{c1}}{\mathrm{d}t} = \frac{i_{L1}}{C_1}(1-u_1) - \frac{i_{L2}}{C_1} \quad (3)$$

$$\frac{\mathrm{d}v_{c2}}{\mathrm{d}t} = \frac{i_{L2}}{C_2}(1-u_2) - \frac{v_{c2}}{RC_2} \quad (4)$$

where for the first stage (resp. second stage) $u_1 = 1$ when the switch S_1 (resp. S_2) is closed and $u_1 = 0$ when the switch S_1 (resp. S_2) is open, and V_g is a constant source voltage. All the parameters that appear in (1)-(4) are shown in Fig. 3.

2.1.2. Equivalent control variables

The equivalent control variables are obtained by imposing that the trajectories are evolving on the switching manifolds and therefore one has $s_1(x) = \dot{s}_1(x) = 0$ and $s_2(x) = \dot{s}_2(x) = 0$. Taking into account that the input voltage is constant one has the following set of equations defining the sliding mode dynamics

$$s_1(x) = 0 \qquad s_2(x) = 0 \quad (5)$$

$$\dot{s}_1(x) = -\frac{\mathrm{d}i_{L1}}{\mathrm{d}t} = 0 \quad (6)$$

$$\dot{s}_2(x) = g_2\frac{\mathrm{d}v_{c1}}{\mathrm{d}t} - \frac{\mathrm{d}i_{L2}}{\mathrm{d}t} = 0 \quad (7)$$

Due to the constraints described by (5), the ideal sliding dynamics is 2-dimensional. Only (6) and (7) define the sliding dynamics. Under sliding conditions, the equivalent control variables $u_{eq1}(x)$ and $u_{eq2}(x)$ represent the control laws that describe the behavior of the system restricted to the switching surfaces where the system motion takes place on the average. Hence, from (1)-(4) and (6)-(7), $u_{eq1}(x)$ and $u_{eq2}(x)$ can be expressed as follows

$$u_{eq1} = 1 - \frac{V_g}{v_{c1}} \quad (8)$$

$$u_{eq2} = 1 - \frac{v_{c1}}{v_{c2}}\left(1 + \frac{g_2^2 L_2}{C_1}\right) + \frac{V_g^2}{v_{c1}v_{c2}}\frac{L_2 g_1 g_2}{C_1} \quad (9)$$

Note that the equivalent control variables u_{eq1} and u_{eq2} must be bounded by the minimum and maximum value of u [11], [12], i.e

$$0 < u_{eq1}(x) < 1 \quad \text{and} \quad 0 < u_{eq2}(x) < 1 \quad (10)$$

2.1.3. Sliding mode conditions

By imposing the existence conditions given by (10), the sliding domain in the parameter and in the state spaces can be obtained. For instance, in the plane (v_{c2}, v_{c1}) and based on (8)-(9) and (10), the sliding mode regime will exist provided that $V_g < v_{c1} < v_{c1L}$ where the critical value v_{c1L} is given by

$$v_{c1L} = \frac{v_{c2}C_1 + \sqrt{v_{c2}^2 C_1^2 + 4V_g^2 L_2 g_1 g_2 (C_1 + L_2 g_2^2)}}{2(C_1 + g_2^2 L_2)} \quad (11)$$

It should be noted that theoretically, other boundaries are also exist but the one expressed by (11) is the most restrictive. Introducing (8) and (9) in (1)-(4) and considering (5)-(7) will result in the following model for ideal sliding dynamics

$$\frac{\mathrm{d}v_{c1}}{\mathrm{d}t} = \frac{g_1 V_g^2}{C_1 v_{c1}} - \frac{g_2 v_{c1}}{C_1} \tag{12}$$

$$\frac{\mathrm{d}v_{c2}}{\mathrm{d}t} = \frac{v_{c1}^2}{v_{c2}}\left(\frac{g_2}{C_2}\left(1 + \frac{g_2^2 L_2}{C_1}\right)\right) - \frac{g_2}{C_2}\frac{V_g^2}{v_{c2}}\frac{g_1 g_2 L_2}{C_1} - \frac{v_{c2}}{RC_2} \tag{13}$$

The next step in our study will be the determination of the equilibrium point of the model defined in (12) and (13).

2.1.4. Equilibrium point

The equilibrium point can be obtained by forcing the time derivative of the state variables of the reduced order model to be null. From (12), (13) and taking into account (5), the equilibrium point of the ideal sliding dynamics is given by

$$x^* = [V_{c1}, V_{c2}]^\top = V_g\left[\sqrt{\frac{g_1}{g_2}}, \sqrt{Rg_1}\right]^\top \tag{14}$$

From the equilibrium point and considering that the output power is equal to the input power and that the input voltage in a boost converter is less than its output voltage, the following constraint on the parameters must be imposed

$$g_1 > g_2 \quad \text{and} \quad g_1 > \frac{1}{R} \tag{15}$$

2.1.5. Stability analysis

The expressions (12)-(13) that represents the ideal sliding dynamics are nonlinear. In order to study the stability of the system, (12)-(13) are first linearized around the equilibrium point x^* given by (14). The corresponding Jacobian matrix $\mathbf{J}$ can be expressed as follows

$$J = \begin{pmatrix} -\dfrac{2g_2}{C_1} & 0 \\ \dfrac{2\sqrt{g_2}(C_1 + L_2 g_2^2)}{\sqrt{R}C_1 C_2} & -\dfrac{2}{RC_2} \end{pmatrix} \tag{16}$$

The characteristic polynomial equation of the linearized system can be obtained from $\det(\mathbf{J} - s\mathbf{I}) = 0$, Developing this equation, the characteristic polynomial equation can be written in the following form:

$$(s + \frac{2g_2}{C_1})(s + \frac{2}{RC_2}) = 0 \tag{17}$$

whose roots $-2g_2/C_1$ and $-2/(RC_2)$ are located in the left half plane and hence, the system is asymptotically stable.

2.2. the Z-source converter under sliding mode-control

Fig. 4 depicts the circuit description corresponding to the Z-source converter under SMC. A single control variable is used to drive the switch of the Z-source converter. The inductor current i_{L1} can be considered as an input current for the same converter. The sliding surface imposes that the input current of the converter i_{Lz1} is proportional to the input voltage of the Z-source converter. The sliding surface can be described with the switching function: $s(x) = gV_g - i_{Lz1}$. In steady-state $s(x) = 0$, i.e., $I_{Lz1} = gV_g$. To use the symmetrical behavior of Z-source structure, the Z-source capacitors (C_z) are set equal to each other and Z-source inductors, (L_z) are chosen such as thei inductance values and sizes are the same. Then, by the symmetry, the voltage waveforms on the Z-source inductors are identical. The current waveforms through Z-source capacitors are also identical.

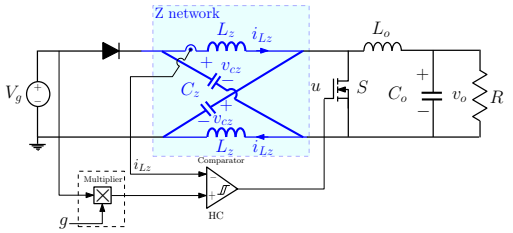

Figure 4. The schematic diagram for a Z-source converter under SMC.

2.2.1. Switched model

By applying standard KVLs and KCLs to the circuit depicted in Fig.4, the Z-source converter can be represented by the following differential equations

$$\frac{\mathrm{d}i_{Lz1}}{\mathrm{d}t} = \frac{(1-u)V_g}{L_z} + \frac{(u-1)v_{cz1} + uv_{cz2}}{L_z} \tag{18}$$

$$\frac{\mathrm{d}i_{Lz2}}{\mathrm{d}t} = \frac{(1-u)V_g}{L_z} + \frac{(u-1)v_{cz2} + uv_{cz1}}{L_z} \tag{19}$$

$$\frac{\mathrm{d}i_{Lo}}{\mathrm{d}t} = \frac{(u-1)V_g - i_{Lo}R}{L_o} + \frac{(1-u)(v_{cz1} + v_{cz2})}{L_o} \tag{20}$$

$$\frac{\mathrm{d}v_{cz1}}{\mathrm{d}t} = \frac{(1-u)i_{Lz2} - ui_{Lz1}}{C_z} - \frac{(1-u)i_{Lo}}{C_z} \tag{21}$$

$$\frac{\mathrm{d}v_{cz2}}{\mathrm{d}t} = \frac{(1-u)i_{Lz1} - ui_{Lz2}}{C_z} - \frac{(1-u)i_{Lo}}{C_z} \tag{22}$$

where V_g is a voltage source which is considered constant. All the other parameters that appear in (18)-(22) are shown in Fig. 4. The signal u is the control variable used to drive the switch of Z-source converter. $u = 1$ during the period T_{ON} and $u = 0$ during the period T_{OFF}.

2.2.2. Equivalent control variable

Following a similar procedure to that of the previous section, the equivalent control variable for the Z-source converter under SMC can be obtained by taking into account the following set of equations defining the sliding mode dynamics

$$s(x) = gV_g - i_{Lz1} = 0 \tag{23}$$

$$\dot{s}(x) = -\frac{\mathrm{d}i_{Lz1}}{\mathrm{d}t} = 0 \tag{24}$$

From (18)-(22) and (23)-(24), the following expression is obtained for the equivalent control variable $u_{eq}(x)$

$$u_{eq} = \frac{v_{cz1} - V_g}{v_{cz1} + v_{cz2} - V_g} \tag{25}$$

Note that $u_{eq}(x)$ must be bounded by the minimum and maximum value of u [11], [12], i.e

$$0 < u_{eq}(x) < 1 \tag{26}$$

2.2.3. Sliding mode conditions

By imposing the existence conditions given by (26), the sliding domain in the parameter and in the state spaces can be obtained. For instance, in the plane (i_{Lo}, v_{cz1}) and based on (25) and (26), the sliding mode regime will exist provided that $V_g < v_{cz1}$.

Substituting (25) in (18)-(22) and taking into account (23)-(24), the following ideal sliding dynamics reduced-order model is obtained

$$\frac{\mathrm{d}i_{Lz2}}{\mathrm{d}t} = \frac{v_{cz2}-v_{cz1}}{L_z} \tag{27}$$

$$\frac{\mathrm{d}i_{Lo}}{\mathrm{d}t} = \frac{v_{cz1}-i_{Lo}R}{L_o} \tag{28}$$

$$\frac{\mathrm{d}v_{cz1}}{\mathrm{d}t} = \frac{v_{cz1}(i_{Lz2}-i_{Lo})+gV_g(V_g-v_{cz2})}{(v_{cz1}+v_{cz2}-V_g)C_z} \tag{29}$$

$$\frac{\mathrm{d}v_{cz2}}{\mathrm{d}t} = \frac{v_{cz1}(gV_g-i_{Lo})+i_{Lz2}(V_g-v_{cz2})}{(v_{cz1}+v_{cz2}-V_g)C_z} \tag{30}$$

2.2.4. Equilibrium point

The equilibrium point can be obtained by forcing the time derivative of the state variables of the averaged model to be null. From (27)-(30) and taking into account Eq. (24), the equilibrium point of the ideal sliding dynamics is given by

$$x^* = [I_{Lz2}, I_{Lo}, V_{cz1}, V_{c2z}]^\top = V_g\left[g, \sqrt{\frac{g}{R}}, \sqrt{Rg}, \sqrt{Rg}\right]^\top \tag{31}$$

The control variable u_{eq} at the equilibrium point can be obtained by substituting (31) in (25). In doing so, one obtains the following steady state value U_{eq} of the control variable u_{eq}

$$U_{eq} := u_{eq}(x^*) = \frac{\sqrt{R\,g}-1}{2\sqrt{R\,g}-1} \tag{32}$$

As we mentioned before in (10) that U_{eq} is bounded between 0 and 1, the following condition should be fulfilled

$$\sqrt{Rg} > 1 \tag{33}$$

2.2.5. Stability analysis

In order to study the stability of the system, the nonlinear model (27)-(30) is linearized around the equilibrium point x^* given by (31). The stability of the linearized system can be studied by using the Jacobian matrix $\mathbf{J}$ corresponding to (27)-(30) and evaluating it at the equilibrium point x^*. This matrix can be expressed as follows

$$\mathbf{J} = \begin{pmatrix} 0 & 0 & -\frac{1}{L_2} & -\frac{1}{L_2} \\ 0 & -\frac{R}{L_o} & \frac{1}{L_o} & 0 \\ a & -a & -b & c \\ d & a & -b & c \end{pmatrix} \tag{34}$$

where the parameters a, b, c and d can be defined as follows

$$a = \frac{-\sqrt{Rg}}{C_z(2\sqrt{Rg}-1)}, \quad d = \frac{\sqrt{Rg}-1}{C_z(2\sqrt{Rg}-1)}, \quad b = \frac{d(\sqrt{\frac{g}{R}}-2g)}{2\sqrt{Rg}-1}, \quad c = \frac{a(\sqrt{\frac{g}{R}}-2g)}{2\sqrt{Rg}-1} \tag{35}$$

The local stability analysis of the system can be carried out by using the characteristic polynomial equation $p(s) = \det(\mathbf{J} - s\mathbf{I}) = 0$ of the linearized system, where $\mathbf{I}$ is the unitary matrix. Developing this equation, $p(s)$ can be written in the following form

$$p(s) = s^4 + a_3 s^3 + a_2 s^2 + a_1 s + a_0 \tag{36}$$

where a_3, a_2, a_1 and a_0 can be defined as follows

$$a_3 = \frac{L_o(b-c)+R}{L_o}, \quad a_2 = \frac{R(b-c)+a}{L_o} + \frac{a-d}{L_z}, \quad a_1 = \frac{a_3(a-d)}{L_z}, \quad a_0 = \frac{((R(b-c)+a)(a-d)}{L_o L_z} \tag{37}$$

Using Routh-Hurwitz criterion, four conditions for stability are obtained, three of them are always fulfilled while another one establishes that for stability to be guaranteed, a certain function c that depends on many parameters of the system must be positive. The expression of $c(R)$ of this condition holds too much space and not included here. However this expression is shown in Fig. 5 in terms of the load resistance. The critical value of the load resistance for stability boundary is about 927 Ω for $R < 927$ the system is stable while for $R > 927$ Ω, the system becomes unstable. In conclusion, while the dual-stage boost converter is stable without any condition, the Z-source converter

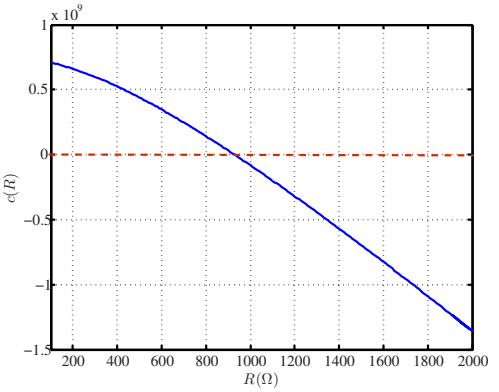

Figure 5. The function $c(R)$ establishing the stability condition with respect to the load resistance R. The system is stable if $c(R) < 0$.

is only stable if a certain condition in terms of the system parameters is fulfilled.

3. Static Performances

The static performances can be represented in terms of many figures of merits. In this paper we consider the efficiency as the main figure of merit to be compared for both systems. Other aspects such as size, weight and cost will be discussed. The efficiency of a switching converter depends mainly on the losses in the parasitic parameters which have been considered ideal in the previous sections. The main losses of the system are due to the inductors (conduction losses), diodes and MOSFETs (conduction/switching losses) while capacitor losses can be neglected because of their small effect. The power lost in the different components of the converter can be expressed as follows

Inductor Losses:

$$P_{L_i} = I_{L_i}^2 R_{L_i} \tag{38}$$

Diode Losses:

$$P_d = V_{D_i} I_{L_i}(1 - D_i) + f_s T_{rD_i} I_{L_i} V_{C_i} + 0.5 f_s T_{rD_i} I_{rD_i} V_{C_i} \tag{39}$$

MOSFET Losses:

$$P_s = I_{L_i}^2 R_{on_i} D_i + 0.5 f_s C_{ds_i} V_{c_i}^2. \tag{40}$$

where R_{L_i} is the inductor DC resistance, R_{on_i} is the ON resistance of the MOSFETs and f_s is the switching frequency. The remaining diode and MOSFET parameters, such as V_{D_i}, T_{rD_i}, I_{rD_i} and C_{ds_i} can be obtained from datasheets. For the Z-source converter, the efficiency obtained with the parameter values used is equal 78% although the system is working with a duty cycle less than 50%. The low value of the efficiency can be attributed to the used three inductors which increases the copper losses. Also, the MOSFET current is equal to the inductor current which increases the switching losses. For the dual-stage boost converter, the efficiency obtained is about 85%. The relatively better efficiency is due to the fact that this system uses only two inductors with different values of currents and two MOSFETs.

The switching current in the first MOSFET is large and its switching voltage is the intermediate voltage v_{c1}. For the second MOSFET, its switching voltage is high 380 V but its switching current is relatively small.

From a size point of view, the Z-source converter has three inductors, three capacitors, one MOSFET and one diode, while the dual-stage boost converter has two inductors, two capacitors, two switches and two diodes. According to this, the size of the dual-stage converter could be larger than the volume of the Z-source converter.

4. Numerical simulations

Table 1. The used parameter values for the dual-stage and the Z-source converters.

V_g	V_{c2}=V_{cz2}	L_1	$L_2 = L_z$	$C_1 = C_2 = C_z$	g =g_1	R
18 V	380 V	500 μH	1 mH	100 μF	0.3 S	1500 Ω

In order to verify the theoretical results predicted in Sections 2 and 3, the Z-source converter and the dual-boost converters have been simulated by using PSIM software with the set of parameter values depicted in Table I.

The Z-source converter under SMC has been simulated to check the previous stability conditions. The system has been checked for two values of the load resistance. Fig. 6(a) shows that the system is stable for load resistance R =300 Ω. The system becomes unstable for load resistance R =1500 Ω as it is depicted in Fig. 6(b) where it can be observed that a small amplitude and low frequency oscillation appears in the inductor currents and the capacitor voltages.

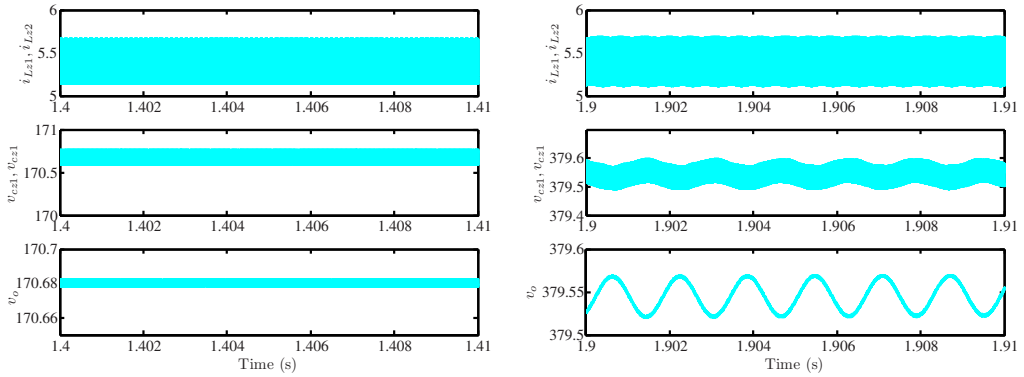

(a) Stable case at load 300 Ω.

(b) Unstable case at 1500 Ω.

Figure 6. The inductor current i_L and the capacitor voltages v_c and v_o of the Z-source converter with g = 0.3.

Similarly, the dual-stage boost converter under SMC has been simulated to check ist stability under input voltage and load variations. Fig. 7(a) shows the effect of the input voltage variation from 18 V to 20 V. As the input voltage increases, the output capacitor voltages and the inductor currents are also increased. Fig. 7(b) shows the response of the system to a step change in the load resistance from 1500 Ω to 750 Ω. In this case, the capacitor voltage v_{c1} and the inductor currents remain constant. In contrast to the Z-source converter, the system remains stable whenever that sliding mode conditions are fulfilled

5. Conclusion

In some PV energy conversion applications, high conversion ratios are needed. Different techniques and converter topologies can be obtained to handle this problem. In this paper, the Z-source converter and a dual-stage boost converter have been compared for their potential use in this kind of applications. The two structures have been analyzed

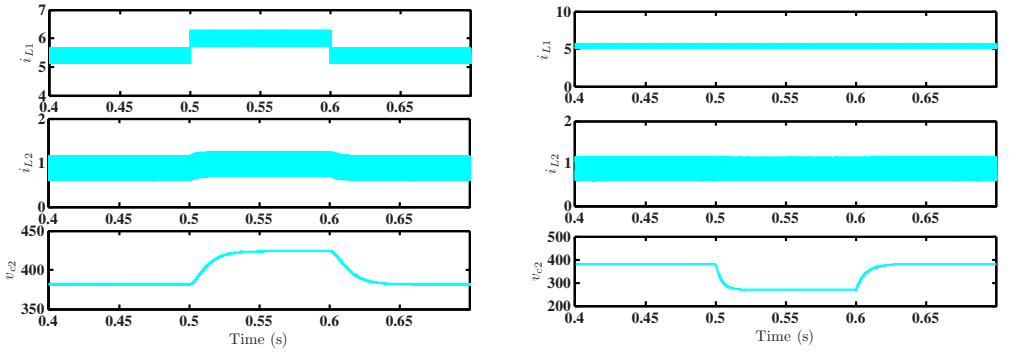

(a) Input voltage change from 18 V to 20 V.

(b) Load change from 1500 Ω to 750 Ω.

Figure 7. The capacitor voltages v_{c2} and v_{c1} and the inductor currents i_{L1} and i_{L2} of the dual-stage boost converter with $g_1 = 0.3, g_2 = 0.008$.

theoretically and by numerical simulations using PSIM software. Large-signal dynamical models and stability analysis of both systems has been presented out to obtain the conditions for sliding motions and for stability boundary in their design parameter space. It has been shown that both systems can be used to solve the problem of achieving high voltage conversion ratio with high efficiency but the dual-stage boost converter outperforms the Z-source converter in terms of both dynamic and static performances. Future works will deal with the experimental validation of the theoretical results and the numerical simulations.

6. Acknowledgements

This work was supported by the Spanish MINECO under grants DPI2010-16481, DPI2010-16084 and CSD2009-00046.

References

[1] A. Cellatoglu and K. Balasubramanian, "Renewable energy resources for residential applications in coastal areas: A modular approach," in *42nd Southeastern Symposium on System Theory (SSST)*, 2010.
[2] S. Luo and I. Bataresh, "A Review of distributed power systems part I: DC distributed power system," *IEEE Aerospace and Electronic Systems Magazine*, vol. 20, no. 8, pp. 5–16, 2005.
[3] B. Fahimi, A. Kwasinski, A. Davoudi, R. S. Balog, and M. Kiani, "Powering a more electrified planet," *IEEE power and energy magazine*, no. 2, pp. 54–64, 2011.
[4] A. Sannino, G. Postiglione, and M. H. J. Bollen, "Feasibility of a DC network for commercial facilities," *IEEE Transactions on Industry Applications*, vol. 39, no. 5, pp. 1499–1507, 2003.
[5] D. Nilsson, *DC distribution systems*. PhD thesis, Chalmers University of Technology, Sweden, 2005.
[6] G. R. Walker and P. C. Sernia, "Cascaded DC-DC converter connection of photovoltaic modules," *IEEE Transactions on Power Electronics*, vol. 19, no. 7, pp. 1130–1139, 2004.
[7] A. I. Bratcu, I. Munteanu, S. Bacha, D. Picault, and B. Raison, "Cascaded DC-DC converter photovoltaic systems: power optimization issues," *IEEE Transactions on Industrial Electronics*, vol. 58, no. 2, pp. 403–411, 2011.
[8] X. Yang, H. Zhang, and X. Ma, "Modeling and stability analysis of cascade buck converters with N power stages," *Mathematics and Computers in Simulation*, vol. 80, no. 3, pp. 533–546, 2009.
[9] P. F. Z. Zheng, "Z-source Inverter," in *37th Annual Meeting. Conference Record of the Industry Applications Conference (IAS)*, 2002.
[10] L. Jingbo, R. Autom, and Milwaukee, "Dynamic modeling and analysis of Z source converter-derivation of AC small signal model and design-oriented analysis," *IEEE Transactions onPower Electronics*, vol. 22, no. 5, pp. 1786– 1796, 2007.
[11] V. I. Utkin, *Sliding modes and their application in variable structure systems*. MIR Publishers, 1978.
[12] P. Mattavelli, L. Rossetto, G. Spiazzi, and P. Tenti, "General-purpose sliding-mode controller for DC/DC converter applications," in *24th Annual IEEE Power Electronics Specialists Conference, (PESC)*, pp. 609 – 615, 1993.